Dissociation of Highly Excited NO_2 Induced by Collisions with Ar, CO, and O_2

A. Sanov, C. R. Bieler, and H. Reisler*

Department of Chemistry, University of Southern California, Los Angeles, California 90089-0482

Received: July 21, 1994; In Final Form: September 29, 1994[⊗]

The gas-phase collision-induced dissociation (CID) of highly excited, mixed $^2A_1/^2B_2$ states of NO_2 with Ar, CO, and O_2 is studied in crossed beams experiments with state-resolved detection of products. Both the internal and translational energy of the reactants are varied independently. The state-specific relative yield of the NO product as a function of the initial NO_2 excitation is reported for excitation energies $h\nu$ from dissociation threshold D_0 to $D_0 - h\nu = 1000$ cm^{-1}. The relative collision energies are 750−2400 cm^{-1}. The structure of the CID yield spectrum is similar to that observed in the fluorescence excitation spectrum of NO_2, and the scaling of the collisional energy transfer efficiency can be described by an exponential decay law. NO is detected using laser ionization, and rotational and spin−orbit distributions are determined. CID is described fairly well by assuming a unimolecular decomposition (UMD) of NO_2, collisionally excited to a range of excess energies above D_0 with excitation probability determined by the exponential gap law. The average energy transferred per activating collision is in the range 110−310 cm^{-1}, dependent on both the relative collision energy and the nature of the collider. Higher product spin−orbit excitations are observed with CO and O_2 than with Ar which suggests a stronger exit−channel interaction with these colliders.

I. Introduction

Understanding collision-induced dissociation (CID) of polyatomic molecules is of fundamental importance to the understanding of unimolecular and recombination processes. In thermal, collisional environments both processes reflect a delicate balance between activating and deactivating collisions.[1] For example, in unimolecular reactions the Lindemann mechanism is based on the assumption that strong collisions can activate molecules to energies above dissociation threshold, transferring large amounts of energy in a single collision.[2] In recombination reactions, the stability of the product depends on the efficiency of the deactivating collisions, and efficient upward energy transfer may reduce the observed net recombination rate. In addition, molecules with high internal energy may have sufficient energy to participate in chemical reactions. Thus, issues of energy transfer are central to any modeling of unimolecular and bimolecular reactions in collisional environments. The importance of these processes has been recognized for many years, and the history of studying energy transfer is as long as that of unimolecular reactions.[3,4]

Most of the studies on energy transfer have been concerned with molecules with low amounts of vibrational energy. Of the relatively few studies that have dealt with highly vibrationally excited polyatomic molecules, the majority examined relaxation, that is downward (deactivating) collisions. The most extensively studied triatomic molecule is highly excited NO_2 (hereafter denoted NO_2*).[5−9] Studies of its relaxation yielded the average energy transferred per collision as a function of excitation energy and the nature of the collider. However, recent results provide state-resolved information on NO_2* collisional relaxation.[6,9]

Theoretical investigations of energy transfer at high internal energies are scarce as well and involve mainly trajectory calculations. Studies of small molecules emphasize issues such as strong *vs* weak collisions and the importance of V−V and V−R transfer,[10−12] while calculations centered on large molecules demonstrate the importance of "chattering" collisions.[13,14] The latter showed that, in large molecules, an atomic collider can collide sequentially with more than one atom in the excited molecule in the course of a single collision, undergoing several energy-changing events. The net energy transferred can be different than that in each one of these encounters. Such chattering collisions make the duration of the collision rather long. To our knowledge, the only theoretical work that treats explicitly the collisional dissociation of a triatomic molecule with substantial internal energy concerns the CID of HO_2* by He to yield H + O_2 or OH + O.[15] This study, which uses trajectory calculations, shows that the CID cross section is smaller when HO_2* is rotationally "cold" than when it was "hot". The authors suggest that the CID of rotationally hot HO_2* can be modeled by a strong collision mechanism, while rotationally cold HO_2* is better modeled by a weak collision approximation.

CID studies are unique because they only sample upward collisions that result in fragmentation. Although CID is used routinely in ion−molecule reactions, few studies of gas-phase CID of neutral molecules have been reported. CID of alkali halides with rare-gas colliders was shown to generate ion pairs at collision energies up to 6 eV.[16,17] Laser excitation into upper electronic states was used by Leone and co-workers to study the CID of Br_2, which dissociated following collision-induced curve crossing onto a repulsive electronic surface.[18] Related experiments of CID on surfaces have shown a sharp dependence of the CID yield on translational energy and the stiffness of the surface, and product energy distributions that could be well described by statistical theories of unimolecular decay.[19−21] We believe that studies of CID of triatomic molecules should be particularly revealing. The density of states of these molecules and the number of degrees of freedom are sufficiently large to make the probability of CID substantial, and the internal energy distributions in the products should shed further light on the CID mechanisms. From a theoretical standpoint they may be tractable, and realistic potential energy surfaces can be constructed.

Recently, we have reported the first study of gas-phase CID of NO_2* by Ar carried out in crossed molecular beams with a

[⊗] Abstract published in *Advance ACS Abstracts,* May 1, 1995.

0022-3654/95/2099-7339$09.00/0

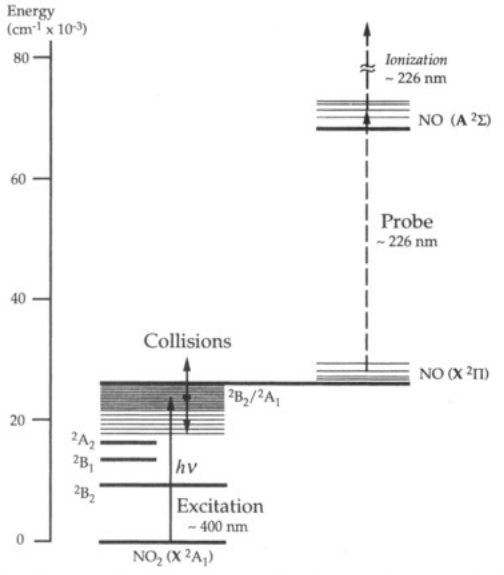

Figure 1. Energy diagram showing the three major steps in the CID of NO_2*: laser excitation ($NO_2 \rightarrow NO_2$*); collisional excitation (or deactivation) of NO_2* followed by dissociation of NO_2 molecules excited above D_0, NO_2*‡; detection of NO($^2\Pi$) products. Also shown are the origins of the relevant NO_2 electronic states.

good selection of the internal and translational energies of the reactants.[22] NO_2 was excited by a pulsed laser to selected energies below the dissociation threshold, $D_0 = 25\ 130\ cm^{-1}$,[23] and the relative energy of collisions with Ar was defined by the molecular beam expansion conditions. Thus, we could study separately the roles of internal and translational energy in promoting dissociation. Figure 1 depicts schematically the relevant electronic states of NO_2 and the three major steps of the CID experiment (i.e., laser excitation of NO_2, collisional dissociation, and detection of NO products). NO was monitored state-selectively, and its relative yield was determined as a function of the internal energy in NO_2. From these data we estimated the average energy transferred per collision and obtained the rotational and spin−orbit distributions in NO. The CID yield was found to obey an exponential gap law as is characteristic of adiabatic collisions.

In this paper we give a full account of our CID studies with Ar, extend them to a broader range of internal and translational energies, and include also CO and O_2 colliders. Diatomic colliders do not have many internal degrees of freedom, and in that respect their behavior is not expected to be very different from the inert gas. However, with highly excited NO_2*, reactive channels become energetically possible that may yield O_3 and CO_2 products in collisions with O_2 and CO, respectively. Thus, the influence of attractive interactions, or even reactions, on the collision outcomes can be examined. We also compare the results of the NO_2 + Ar CID at two markedly different collision energies.

NO_2 provides an excellent prototypical system for studying CID of highly internally excited molecules. It can be optically excited almost continuously to levels around D_0 by using excitation into the mixed $^2B_2/^2A_1$ state (see Figure 1).[24−26] Although only the excited $^2B_2$ state carries oscillator strength, it is vibronically coupled to the ground $^2A_1$ state. This strong coupling induces mixing among many zero-order states, and vibronic chaos has been established at energies above 16 000 cm^{-1}.[26] Thus, even in the absence of collisions, the prepared molecular eigenstates are mixed states which, on the basis of consideration of density of states, have >80% ground state character. Since only the $^2B_2$ state carries oscillator strength, the fluorescence lifetime of NO_2 is much longer than the radiative lifetime predicted from the absorption coefficient, giving rise to the well-known Douglas effect.[27] Near D_0, the lifetimes of the excited NO_2 molecules are >50 μs,[28] and thus they can be transported in the molecular beam over large distances without substantially losing their excitation. As discussed later, this fact proves to be of crucial importance to the success of the CID experiments.

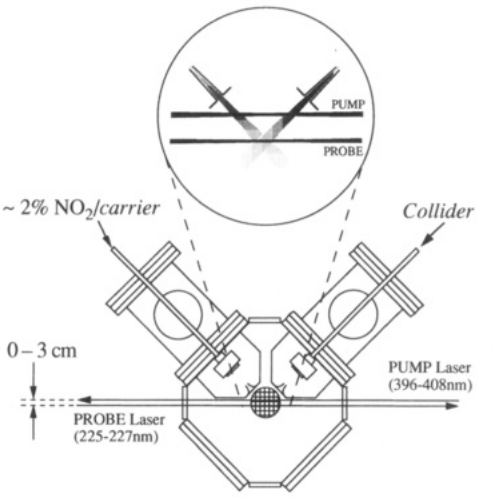

Figure 2. Experimental arrangement employed in the CID experiment. The shaded area is the ion-optics region of the mass spectrometer mounted perpendicularly to the plane of the molecular and laser beams. The inset shows the configuration of the lasers and molecular beams.

The existence of excited electronic states in NO_2 which are strongly coupled to the ground state is the key to our ability to excite these molecules efficiently to high vibrational levels of the ground state. On the other hand, this fact also complicates interpretations, since the electronically excited states may participate in the energy transfer. In studies of the relaxation of NO_2, it was found that the energy transfer probability increases strongly above the origin of the electronically excited state.[7,29] In this regard, NO_2 may prove to be somewhat special. However, in the CID studies reported here, no indication of the importance of electronic effects can be obtained.

Our results show that CID is fairly efficient near D_0, but the yield decreases exponentially when the amount of transferred energy required to reach D_0 increases. We model the CID by assuming separate steps for collisional activation and unimolecular decay. The experimental results are in reasonable agreement with such a mechanism but show evidence of exit-channel interactions with the collider.

II. Experimental Section

1. Experimental Arrangement. The experiments are performed in a crossed beams apparatus consisting of a main collision chamber and two adjacent molecular beam source chambers (Figure 2). The two differentially-pumped pulsed molecular beams are expanded into the interaction chamber through piezoelectrically actuated pulsed nozzles (0.5-mm aperture, ~150-μs opening time)[30] and 3-mm homemade skimmers. The first beam consists of NO_2 seeded in a carrier gas (He or Ar), and the second beam is neat collider gas (Ar, CO, or O_2). The beams travel approximately 50 mm from the skimmer to the center of the chamber and intersect at 90°, creating an overlap region of ~1 cm^3. The vacuum chamber base pressure is ~5 × 10^{-7} Torr, and under typical operating conditions (10-Hz pulse repetition rate, 1.5-atm backing pressure) the pressure in the collision chamber is <2 × 10^{-5} Torr.

An excimer-laser pumped dye-laser system is utilized to excite the expansion-cooled NO_2 in the beam into mixed $\tilde{A}^2B_2/$

$\tilde{X}^2A_1$ molecular eigenstates. The excitation laser beam (15-ns duration, ~4-mJ energy) intersects the NO_2 beam several centimeters away from the skimmer before the center of the collision region (see inset in Figure 2). The separation between the excitation laser beam and the probe beam can be varied in the range 0−3 cm. The excitation wavelength is varied from 396 to 414 nm to cover the energy range from 100 cm^{-1} above D_0 to 1000 cm^{-1} below it. The output from a second, similar laser system is frequency doubled and then used as the probe radiation. The probe beam (~226 nm; 15-ns duration; ~150-μJ energy) crosses the two molecular beams at the center of the collision region. The excitation and probe laser beams are loosely focused with 1-m-focal length lenses to approximately 2- and 1-mm spot sizes, respectively, and counterpropagate in the plane of the molecular beams, intersecting them at 45° and 135°.

2. Molecular Beam Expansion and Kinetic Energy Control. The 2.2% NO_2/carrier gas mixture is prepared by bubbling the carrier gas at 1.5 atm over NO_2 kept at the *o*-xylene/liquid nitrogen slush temperature of −29 °C. The rotational temperature of NO_2 was estimated from the rotational distribution of background NO($^2\Pi_{1/2}$) in the NO_2 beam. Only the three to four lowest rotational states of NO(v=0) have significant populations, corresponding to a temperature <5 K. The NO_2 temperature is not expected to exceed the measured NO temperature,[31] and clustering of NO_2 in the diluted beam is estimated to be <10%.

In the absence of a velocity slip between the carrier gas and NO_2, the final incident energy E_{inc} and the corresponding velocity v of a molecule of mass M in an expanded seeded molecular beam is determined by energy conservation:[32]

$$E_{inc} = \frac{Mv^2}{2} = \frac{M}{\langle m \rangle}\int_{T_{rot.}}^{T} \langle c_p \rangle \, dT \cong \frac{M}{\langle m \rangle}\langle c_p \rangle (T - T_{rot.}) \qquad (1)$$

where $\langle m \rangle$ and $\langle c_p \rangle$ are the average mass and the constant pressure heat capacity of the gas mixture and T is the nozzle temperature. For better accuracy, some of the beam velocities were measured directly by photodissociating NO_2 in the beam at λ = 396.7 nm, the threshold for production of NO ($^2\Pi_{1/2}$;v=0;J=5.5), and detecting NO(J=5.5) with the delayed probe laser beam focused at various distances from the pump beam, downstream from the molecular beam. The experimental arrangement was similar to that shown in Figure 2, the only difference being that the second molecular beam (the collider) was not used. At λ = 396.7 nm, NO(J=5.5) is produced with nearly zero kinetic energy with respect to the parent molecule and propagates with the velocity of the molecular beam. Thus, the beam velocity can be determined by measuring the delay between the excitation and probe laser pulses, adjusted to maximize the NO(J=5.5) signal, as a function of the spatial separation between the two laser beams. The velocity of the Ar collider beam was approximated by the measured velocity of a 2.2% NO_2/Ar mixture. The velocities of the other colliders were estimated from eq 1. The measured and calculated velocities along with the relative collisional energies are summarized in Table 1.

An attempt was made to employ H_2 as a carrier gas in order to generate higher kinetic energies of NO_2. However, a velocity slip in the 2.2% NO_2/H_2 beam due to the poor H_2/NO_2 collision efficiency prevented a significant rise in the NO_2 velocity, as compared to the He carrier. For this reason, H_2 as a carrier gas was not used in the CID experiments.

The molecular beam densities are important in determining single-collision conditions. Under our expansion conditions, the number densities of the NO_2/carrier and collider beams in the center of the chamber are estimated at $\sim 10^{13}-10^{14}$ molecules·cm^{-3}. At these number densities, a rough estimate gives a mean free path of the NO_2 molecules of a few centimeters corresponding to nearly single-collision conditions.

TABLE 1: Velocities of the Molecular Beams and Relative Collision Energies

beam components	beam velocity (m·s^{-1}) calcd	beam velocity (m·s^{-1}) exptl	relative collision energy (cm^{-1}) NO_2−Ar	NO_2−CO	NO_2−O_2
2.2% NO_2/He	1570	1510 (±5%)	2400[a]	2100[b]	2200[b]
2.2% NO_2/Ar	549	655 (±5%)	750[a]	750[b]	760[b]
100% Ar	547	635 (±5%)			
100% CO	774				
100% O_2	724				

[a] Estimated using the experimentally measured beam velocities. [b] Estimated using the experimentally measured NO_2 beam velocity and the calculated (by eq 1) velocity of the collider beam.

3. Detection of CID Products. The CID signal was observed by focusing the probe laser beam at the center of the molecular beam intersection region while the excitation laser beam intersected the NO_2 beam ~3 cm upstream along the supersonic beam, before the molecules enter the interaction region. The 3-cm separation between the excitation and probe laser beams required a ~20-μs delay between firing the lasers to allow NO_2*/He the travel time required to reach the collision region. The long lifetime of NO_2* assured that a significant portion of the NO_2* molecules remained in the excited state when the molecules arrived at the interaction region.

NO was detected state-selectively by resonant 1 + 1 (one-frequency) multiphoton ionization (REMPI) via the $A^2\Sigma^+ \leftarrow X^2\Pi$ transition. Due to poor Franck−Condon overlap,[33a] the ionization cross section of the A state at 226 nm is much smaller than that for the $A^2\Sigma^+ \leftarrow X^2\Pi$ transition requiring near saturation of the A ← X transitions. The NO product state distributions were extracted from the REMPI spectra by assuming that the transitions are totally saturated, as determined from the analysis of room temperature samples and the results reported elsewhere.[33b]

The REMPI intensity is proportional to the number density of the NO molecules. Since NO is produced in a limited region of space, molecules with higher kinetic energy recoil out of the detection region faster than slower ones and, consequently, the effective number density of the "fast" NO product may be smaller than that of the "slow" molecules. Thus, the detection sensitivity for different quantum states of NO might be different, with more favorable detection conditions for the higher internally excited product molecules. However, in our experiments, due to the high velocity of the molecular beams, the differences in the *lab* velocities of the detected NO(J) products are relatively small, and thus corrections for flux/density transformation were not attempted.

The NO^+ ions were detected mass-selectively by a 1-in. microchannel plate (MCP) detector (Galileo Electro-Optics Corp. Model FTD2003) located at the end of a home-built Wiley-McLaren time-of-flight (TOF) mass spectrometer[33c] which was mounted above the center of the collision chamber, perpendicular to the plane of the molecular and laser beams. The mass resolution ($m/\Delta m \sim 20$) allows for discrimination between NO_2^+ (see section II.4) and NO^+ ions, thereby improving the detection selectivity. From considerations of the geometry of the TOF spectrometer and the dimension of the detector, we deduce that all ions formed in the center of the beam interaction region should be detected.[33c]

The signal from the MCP was further amplified and collected in a fast transient digitizer (LeCroy Model TR8818A) for

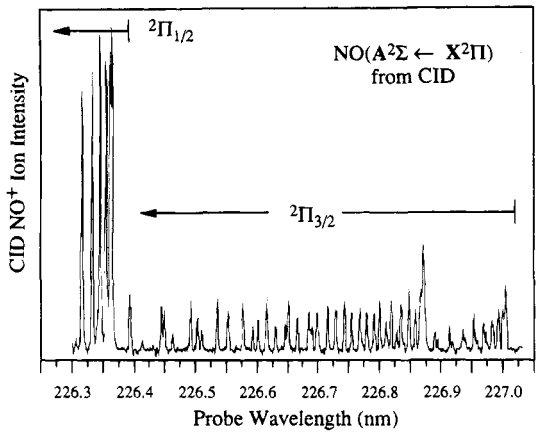

Figure 3. Typical example of the final CID NO spectrum obtained in the NO_2/He + Ar experiment (all background signals are subtracted). The spectrum is obtained by REMPI, via the $A^2\Sigma(v=0) \leftarrow X^2\Pi(v=0)$ transition.

temporary storage and subsequent transfer to the computer. A digital delay generator (Standard Research Systems Inc. Model DG-535) was used for establishing the triggering sequence for the various components of the experimental arrangement. Data processing included signal averaging (at 10 shots per laser grating step) and shot-to-shot normalization of the signals using photodiodes (UDT Sensors Inc. Model UV 1002) to monitor the excitation and probe pulse energies.

4. Interfering Effects. Several competing processes and background signals must be considered in the data analysis, the most important being signals from background NO and from NO products obtained via photodissociation of rotationally hot ground state NO_2. First, the signal due to *background* NO in the NO_2 beam has to be subtracted. Owing to surface catalyzed decomposition of NO_2, small NO concentrations are always present in the molecular beam. Expansion-cooling and skimming ensures that the NO background is at $T_{rot.} < 5$ K, and only NO molecules in the $^2\Pi_{1/2}$ state with $J \leq 3.5$ have significant populations. Nonetheless, in a crossed beams experiment the background NO in low rotational states is collisionally scattered into higher-J states. To subtract the signals due to the background NO and its rotationally inelastic scattering, both the collider gas nozzle and the excitation laser were operated in an *on/off* mode. Subtracting the signal obtained with the collider nozzle off (no collisions) allowed the subtraction of unscattered NO background and yielded the total collision-induced signal. Subtracting the collision-induced signal obtained with the excitation laser off (i.e. the scattered NO contaminant) from the total collision-induced signal obtained with the excitation laser on yielded the CID signal. A typical example of the final CID NO $^2\Pi_{3/2}$ spectrum obtained in the 2.2% NO_2/He + Ar experiment is shown in Figure 3. The CID signal was larger than the background NO signal by a factor of at least 2. The subtraction of the large background signals resulted in significant uncertainty of the final CID signal, estimated at ±20%; however, the shapes of the product state distributions and yield spectra were reproducible.

A more severe problem may arise due to rotational excitation of ground state NO_2 by collisions with the collider *prior* to laser excitation. Exciting NO_2 several centimeters *before* the collision region helps to minimize this effect greatly, although it cannot eliminate it completely. To illustrate this point, Figure 4a shows the NO_2 dissociation yield spectra obtained by monitoring $NO(^2\Pi_{1/2};J=5.5)$ with the collider pulsed nozzle (neat Ar) on and off, and the excitation and probe laser beams overlapping at the center of the collision region. The large, unstructured

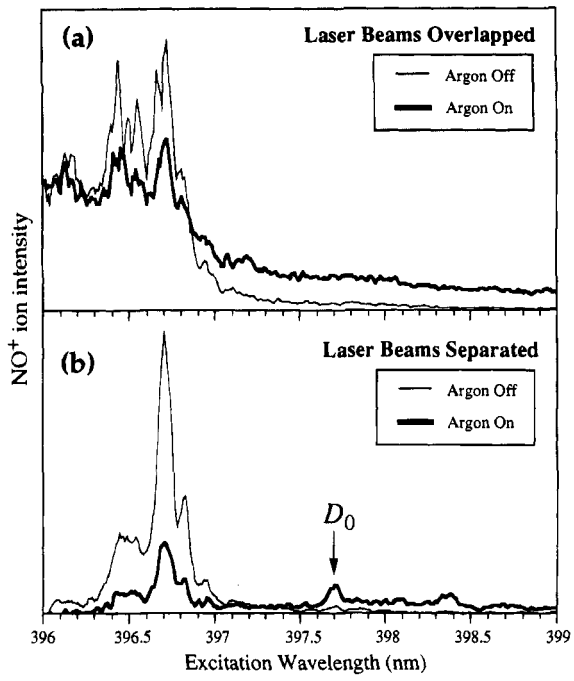

Figure 4. (a) $NO(^2\Pi_{1/2};J=5.5)$ yield obtained in the dissociation of NO_2 as a function of the laser excitation wavelength when the excitation and probe beams are overlapped at the center of the detection region. The thin and thick lines are the spectra obtained with the argon (collider) beam off and on, respectively. (b) Same as in a, except that the excitation laser beam is focused 3 cm away from the probe beam closer to the origin of the NO_2 beam (see Figure 2). The threshold for production of $NO(^2\Pi_{1/2};J=5.5)$ corresponds to the position of the tallest peak at $\lambda = 396.7$ nm. The dissociation threshold is marked by D_0.

collision-induced signal below the threshold for production of $NO(^2\Pi_{1/2})$ in the $J = 5.5$ state is due to photodissociation of NO_2 rotationally excited by collisions with Ar prior to photoexcitation. To decrease the likelihood of such collisional excitation, laser excitation must precede collisions. To achieve this, the excitation laser beam was positioned up to 3 cm away from the center of the chamber, upstream along the NO_2 beam, well outside the molecular beams intersection region (see the inset in Figure 2). Figure 4b shows the NO_2 dissociation yield spectra obtained under the exact same conditions as the spectra in Figure 4a but with the excitation laser beam moved 3 cm away from the center of the collision region. The large decrease of the signal below the $NO(J=5.5)$ photodissociation threshold is due to the diminished contribution from photodissociation of collisionally excited NO_2. The remaining signal below the $NO(J=5.5)$ threshold but above D_0 is due mainly to inelastic scattering of $NO(J<5.5)$ produced by NO_2 photodissociation into the $J = 5.5$ state. The structured signal below D_0 in Figure 4b is attributed to CID, and its spectral structure is discussed in section III.1. We note that even in the absence of collisions with the collider, those NO_2 molecules that are in $N = 2$ and 4 at the 5 K beam temperature will photodissociate when the laser excitation energy is <10 cm^{-1} below D_0. This effect cannot be eliminated but affects only a small region below D_0. In summary, most of the signal due to photodissociation of rotationally excited NO_2 can be eliminated by separating the excitation and probe beams by a few centimeters. The small, remaining signal appears as unstructured background, which can easily be subtracted from the structured CID spectra (e.g., as can be seen in Figure 4b).

The signals in Figure 4a,b *above* the $NO(J=5.5)$ threshold are due to direct photodissociation of NO_2 leading to production of $NO(J=5.5)$. In this wavelength region, the difference between the signals obtained with the collider pulsed nozzle

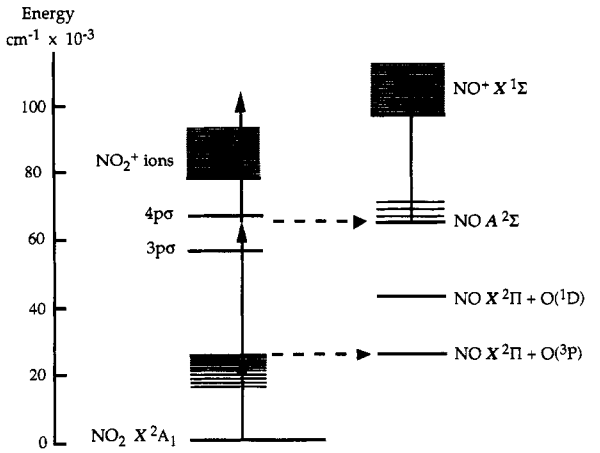

Figure 5. Energy diagram depicting possible interfering multiphoton processes involving NO_2 and NO. Vertical arrows show possible photoexcitation transitions; horizontal dashed arrows indicate NO_2 dissociation pathways. (See the text for details.)

on and off is explained mainly by inelastic scattering of the NO photodissociation product into other rotational states when the collider nozzle is on. The elastic scattering of NO *out* of the detection region is to a large extent counterbalanced by elastic scattering *into* the detection region. Notice in Figure 4b the significant decrease in NO signal intensity above D_0 as the photolysis energy increases. This is best seen by comparing Figure 4b and Figure 4a and is due to the fact that, at laser excitation energies exceeding the threshold for production of NO in the monitored quantum state, NO produced with excess kinetic energy recoils out of the center of the molecular beam and is not overlapped well by the probe beam. Thus, when the excitation and probe beams are separated by 3 cm, there is good discrimination against photolysis products with high recoil energies.

The recoil of translationally hot NO products out of the molecular beam path also minimizes potential interference due to two-photon (~400-nm) dissociation of NO_2, which is quite efficient even at low excitation laser fluences. Since $NO(X^2\Pi)$ created by two-photon dissociation in the excitation region has substantial translational energy, it will recoil out of the molecular beam before it reaches the collision region. In order to increase the discrimination against dissociation products produced with high recoil velocity, the excitation laser was operated with its polarization vector perpendicular to the molecular beam propagation direction. Since the $^2B_2 \leftarrow {}^2A_1$ transition is parallel,[34] the photolysis products will recoil preferably in a direction perpendicular to the plane of the molecular beams and the NO_2 beam velocity. This and other possible interfering photon-induced processes are illustrated in Figure 5.

We also observed a two-frequency two-photon (~400 nm + ~226 nm) dissociation of NO_2 yielding $NO(A^2\Sigma^+)$. This competing pathway is revealed in the NO photoionization spectrum at higher probe energies. Keeping the combined laser frequencies below the $NO_2 \rightarrow NO(A^2\Sigma^+) + O(^3P)$ threshold (69 327 cm^{-1}) eliminated this process. Because of the nonresonant nature of the ionization of $NO(A^2\Sigma^+)$, this process does not exhibit structured absorption and leads to a nearly constant background at higher probe energies. The detectable interference from this pathway confirms that NO_2*, excited 3 cm away from the detection region, does indeed reach the region of interaction with the collider beam.

Finally, we observed a signal due to two-color, three-photon (400 nm + 2 × 226 nm) ionization of NO_2. It is believed that this process proceeds via two intermediate resonances, the first being the $^2A_1/^2B_2$ mixed excited state and the second an excited

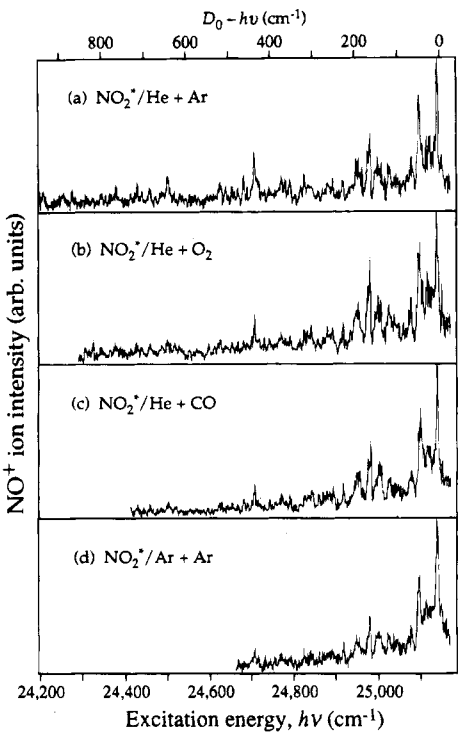

Figure 6. $NO(^2\Pi_{1/2};J=5.5)$ yield from NO_2* CID as a function of NO_2* excitation energy for different colliders and collision energies.

$^2\Sigma_u^+$ Rydberg state, possibly 4pσ. This signal was eliminated by setting the TOF spectrometer to monitor only NO^+ ions.

III. Results

1. CID Yield Spectra. Figure 6 shows the dependence of the CID signal on the initial excitation energy of NO_2*, $h\nu$, for different CID experiments. These spectra, referred to as CID yield spectra, are obtained by scanning the wavelength of the excitation laser below the NO_2 dissociation threshold, D_0, while monitoring the production of $NO(X^2\Pi_{1/2};v=0;J=5.5)$. The intensity of the CID signal decreases as the excitation laser energy is scanned away from the threshold. The decrease is most rapid in the NO_2/Ar + Ar experiment, where the collisional energy is $E_{col} = 750$ cm^{-1}, and the CID signal is detectable to $D_0 - h\nu \sim 500$ cm^{-1}; for $E_{col} = 2100-2400$ cm^{-1} the CID signal is observed to $D_0 - h\nu \sim 1000$ cm^{-1}. Except for their relative intensities, the yield spectra obtained with different colliders and at different collision energies are similar. Likewise, probing different NO product rotational states [e.g. $^2\Pi_{3/2}(J=5.5,6.5)$] results in similar CID yield spectra.

A key observation in identifying the origin of the NO signal is the structure in the CID yield spectra. For comparison, an NO_2 LIF spectrum taken in a companion molecular beam chamber under similar conditions is shown in Figure 7b. The similarities with the CID yield spectra shown in Figure 6a–d are apparent. The yield spectra below D_0 carry the fingerprints of the NO_2 absorption spectrum. This is the primary indication that what is observed is in fact photoexcitation of jet-cooled ($T_{rot.} < 5$ K) NO_2, followed by dissociation. The small NO-(J=5.5) signal at NO_2 excitation energies just above D_0, which is observed in all CID yield spectra (see also Figure 4b), originates from the inelastic scattering of $NO(J<5.5)$ produced by *photodissociation* of NO_2 at energies below the $NO(J=5.5)$ appearance threshold. Just as in CID, this signal is dependent both on the excitation laser and the collider beam and thus cannot be removed by subtraction of the backgrounds in on/off experiments. However, it is limited to the spectral region above D_0 and does not interfere with the CID signal.

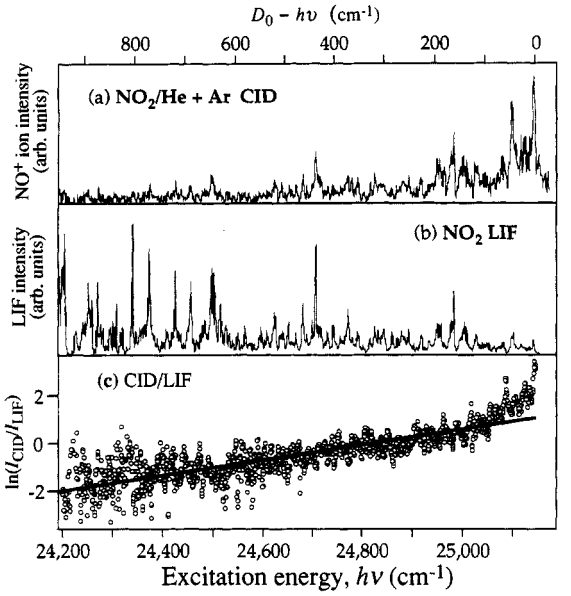

Figure 7. (a) NO($^2\Pi_{1/2}$;J=5.5) CID yield as a function of NO_2* excitation energy in the NO_2/He + Ar experiment (same as in Figure 6a). (b) Jet-cooled NO_2 laser-induced fluorescence (LIF) excitation spectrum. (c) Log plot of the point-by-point ratio of the CID and LIF spectra of NO_2 shown in panels a and b.

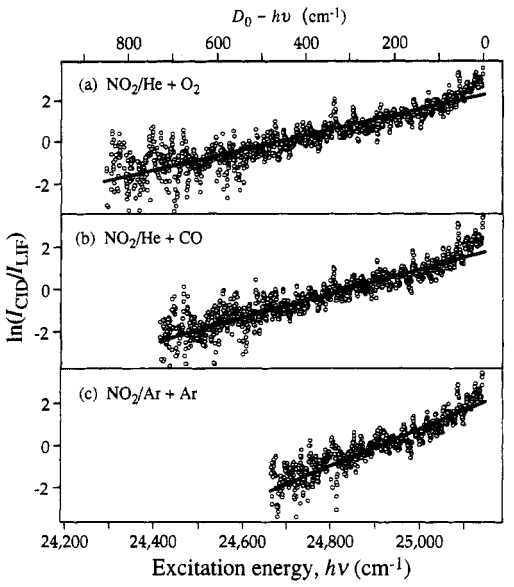

Figure 8. Log plots of the point-by-point ratios of the CID yield spectra shown in Figure 6b–d and the LIF spectrum of NO_2 shown in Figure 7b.

Below D_0, the only significant difference between the NO_2 LIF and CID yield spectra is the relative intensities of the spectral features as the excitation energy is scanned below D_0. This scaling of the CID yield spectra reflects the decreasing energy transfer efficiency as the amount of energy required to produce NO($^2\Pi_{1/2}$;J=5.5) via CID increases. In accordance with the often observed exponential energy gap law for energy transfer,[35] the scaling appears to be exponential in all reported experiments. This observation is illustrated in Figure 7, where panel a shows the CID yield spectrum obtained in the NO_2/He + Ar → NO($^2\Pi_{1/2}$;J=5.5) experiment, panel b shows the jet-cooled NO_2 LIF spectrum, and panel c presents a log plot of the point-by-point ratio of the CID and LIF spectra. Similar plots for the other CID experiments are shown in Figure 8. The linear dependence of the $\ln(I_{CID}/I_{LIF})$ signal on the excitation energy in the investigated energy range confirms that

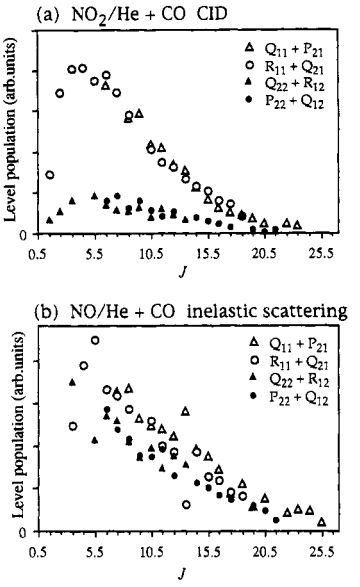

Figure 9. (a) NO($^2\Pi$) rotational level distributions obtained in the NO_2/He + CO CID experiment at NO_2 excitation energy $D_0 - h\nu$ = 160 cm^{-1} (λ = 400.18 nm) and E_{col} = 2100 cm^{-1}. (b) NO($^2\Pi$) rotational level distributions obtained in the inelastic scattering of NO by CO at E_{col} = 1750 cm^{-1}.

TABLE 2: Collisional Energy Transfer Parameters and Measured and Calculated Rotational Temperatures

			NO rotational temp (cm^{-1})		
experiment	E_{col} (cm^{-1})	γ (cm^{-1})	$^2\Pi_{1/2}$ (exptl)	$^2\Pi_{3/2}$ (exptl)	UMD model
NO_2/Ar + Ar	750	114 ± 5	103 ± 10	77 ± 10	80
NO_2/He + CO	2100	175 ± 8	183 ± 15	187 ± 15	150
NO_2/He + O_2	2200	207 ± 10	211 ± 15	173 ± 15	170
NO_2/He + Ar	2400	307 ± 20	256 ± 15	273 ± 25	240

$$I_{CID}(h\nu) \propto I_{LIF}(h\nu) \exp\left(-\frac{D_0 - h\nu}{\gamma}\right) \quad (2)$$

where $h\nu$ is the excitation photon energy. The energy transfer parameter γ is obtained from the linear fits, and the values derived for the different CID experiments are shown in Table 2. In Figures 7 and 8, the nonlinear tails just below D_0 arise from inelastic scattering of NO generated by photodissociation of rotationally excited NO_2 (due to both thermal and collisional excitation, as described in section II.4) into the monitored level—NO(J=5.5). The contribution of this process is significant only within several tens of wavenumbers below D_0, and these sections of the spectra were ignored when fitting the data.

CID near D_0 appears to be quite efficient. Assuming comparable absorption cross sections just below and above D_0, it is found that when probing, for example, NO(J=5.5), the CID signal below D_0 is ~5% of the photodissociation signal near the threshold for formation of NO(J=5.5). This is a significant amount, taking into account that in photodissociation the energy is partitioned into six NO rotational states, whereas in CID NO product states are populated up to $J \sim 25.5$.

2. CID Product State Distributions. Most of the NO product state distributions were obtained by fixing the excitation laser on a prominent peak in the CID yield spectrum at λ = 400.18 nm (160 cm^{-1} below D_0) (see Figure 6) and scanning the probe laser over the NO (A←X) transition. Figure 9a shows a typical rotational distribution obtained in the NO_2/He + CO experiment. Since data analysis was carried out by assuming saturation conditions, only branches with the strongest transitions were used. The peak areas of the R_{11} + Q_{21} and Q_{11} + P_{21} branches were used to derive the J-state populations of the $^2\Pi_{1/2}$

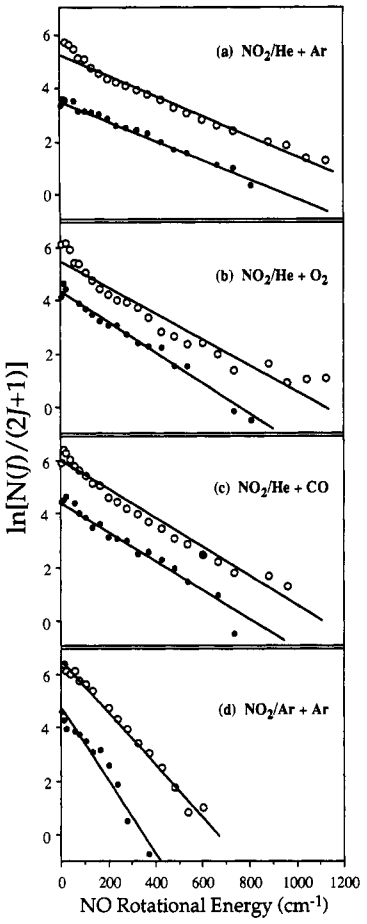

Figure 10. Boltzmann plots of the NO CID product state distributions obtained at NO_2 excitation energy $D_0 - h\nu = 160$ cm^{-1} ($\lambda = 400.18$ nm). The open and closed circles represent NO($^2\Pi_{1/2}$) and NO($^2\Pi_{3/2}$) rotational states, respectively. The populations of different Λ-doublet components are averaged. The temperatures given in Table 2 were obtained from the slopes of the straight lines through the data.

manifold, while those of the $Q_{22} + R_{12}$ and $P_{22} + Q_{12}$ branches were used for the $^2\Pi_{3/2}$ manifold. In the NO_2/He + Ar experiment, the distributions measured at several excitation wavelengths in the range 60−440 cm^{-1} below D_0 were found to be quite similar. Note that for both spin−orbit states there appears to be no preference in the population of the Λ-doublet components.

Figure 10 shows Boltzmann plots [i.e., log(intensity) *vs* rotational energy] of the NO product state distributions obtained in different CID experiments at $\lambda = 400.18$ mm. According to Table 1, the energy (highest J of $^2\Pi_{1/2}$) available to the CID products is 2250 cm^{-1} (35.5), 2050 cm^{-1} (34.5), 1950 cm^{-1} (33.5), and 600 cm^{-1} (18.5) for NO_2/He + Ar, NO_2/He + O_2, NO_2/He + CO, and NO_2/Ar + Ar, respectively.

As seen in Figure 10, the rotational distributions for both NO spin−orbit states appear Boltzmann-like and the rotational temperatures of both spin−orbit states are nearly equal in all cases. Although not all distributions can be equally well described by temperatures, the concept of temperature is useful for characterizing the average energy of the distributions. We have used least squares fits of the form

$$\ln N_\Omega(E_{\text{rot.}}) = a_\Omega - E_{\text{rot.}}/\theta_\Omega, \quad \Omega = {}^1/_2, {}^3/_2 \tag{3}$$

where N_Ω is the population in each spin−orbit state and

$$N_\Omega(E_{\text{rot.}}) = \frac{N_\Omega(J)}{2J+1} \tag{4}$$

TABLE 3: NO($^2\Pi$) Spin−Orbit Ratios from CID and Unimolecular Decomposition

		spin−orbit ratio	
expt	E_{col} (cm^{-1})	exptl	UMD model
NO_2/Ar + Ar	750	0.11 ± 0.03	~0.1
NO_2/He + CO	2100	0.23 ± 0.05	~0.2
NO_2/He + O_2	2200	0.29 ± 0.06	~0.2
NO_2/He + Ar	2400	0.18 ± 0.04	~0.35
NO_2*‡		~0.3[a]	

[a] Obtained in the collisionless unimolecular reaction of NO_2 at excess energies 1900−2100 cm^{-1}, from ref 31.

describes the distribution of the two spin−orbit states in the rotational energy ($E_{\text{rot.}}$) domain. From the fits, the characteristic rotational temperatures θ_Ω listed in Table 2 were obtained.

The least squares fits describe the rotational distributions fairly well, and thus a_Ω and θ_Ω can be used to determine the NO spin−orbit ratios. The total populations of the $^2\Pi_\Omega$ states are given by

$$S_\Omega = \int_0^{\epsilon_\Omega} N_\Omega(E_{\text{rot.}})\, dE_{\text{rot.}}, \quad \Omega = {}^1/_2, {}^3/_2 \tag{5}$$

The upper limits of integration, $\epsilon_{1/2} = E_{\text{avail}}$ and $\epsilon_{3/2} = (E_{\text{avail}} - \epsilon_{s-o})$ for the two spin−orbit states, differ by the value of the NO spin−orbit energy $\epsilon_{s-o} = 123$ cm^{-1}, but since the rotational distributions tail off exponentially up to the available energy, both upper limits can be approximated by infinity. Using the linear fits in eq 3 to characterize the rotational distributions, the populations of the spin−orbit states are given by

$$S_\Omega = \int_0^\infty \exp(a_\Omega - E_{\text{rot.}}/\theta_\Omega)\, dE_{\text{rot.}} = \theta_\Omega \exp(a_\Omega), \quad \Omega = {}^1/_2, {}^3/_2 \tag{6}$$

and the spin−orbit ratio is

$$\frac{^2\Pi_{3/2}}{^2\Pi_{1/2}} = \frac{S_{3/2}}{S_{1/2}} = \frac{\theta_{3/2}}{\theta_{1/2}} \exp(a_{3/2} - a_{1/2}) \tag{7}$$

This approach to the determination of the spin−orbit ratio is advantageous, since it does not require summation of the populations of *all* rotational states, some of which are missing in the experimental distributions due to spectral overlap.

The NO spin−orbit ratios obtained with eq 7 are shown in Table 3. Note that increasing the NO_2−Ar collision energy (NO_2/Ar + Ar *vs* NO_2/He + Ar) significantly increases the CID product spin−orbit excitation. In the NO_2/He + CO, NO_2/He + O_2, and NO_2/He + Ar experiments, the collision energy does not change markedly, but the NO spin−orbit populations nevertheless exhibit a marked dependence on the nature of the collider.

3. Inelastic Scattering of Contaminant NO. NO contaminant is always present in the NO_2 beam, and, in order to obtain accurate CID data, all processes involving NO were monitored on a shot-by-shot basis (see section II.4). Thus, the inelastic scattering of NO was measured simultaneously with CID. Figure 9b shows a typical rotational distribution obtained for inelastic scattering of NO by CO. The values of the characteristic rotational temperatures and spin−orbit ratios for the inelastic scattering of NO are given in Table 4. State-resolved inelastic scattering of NO by Ar has been extensively studied before,[36−38] and our data are in general agreement with the results of these studies. Results on NO inelastic scattering by CO and O_2 have not been reported before and will be described in detail in a separate publication.[39]

TABLE 4: Rotational Temperatures and Spin–Orbit Ratios Obtained in the Inelastic Scattering of NO($^2\Pi_\Omega$)

expt	E_{col} (cm^{-1})	rotational temp (cm^{-1}) $^2\Pi_{1/2}$	rotational temp (cm^{-1}) $^2\Pi_{3/2}$	spin–orbit ratio exptl	spin–orbit ratio statistical
NO/Ar + Ar	600	97 ± 6	118 ± 7	0.17 ± 0.04	~0.3
NO/He + CO	1750	262 ± 16	225 ± 13	0.73 ± 0.15	~0.6
NO/He + O_2	1800	262 ± 16	246 ± 14	0.54 ± 0.11	~0.6
NO/He + Ar	1920	240 ± 14	220 ± 13	0.44 ± 0.09	~0.6

The rotational excitations resulting from the inelastic scattering of NO are comparable to those obtained in CID, although, in the cases of CO and O_2, NO scattering leads to somewhat higher rotational temperatures than CID. Overall, a significantly higher spin–orbit excitation of NO is observed in inelastic scattering compared to CID (compare Figure 9a and Figure 9b), but the general trend in excitation by different colliders appears to be the same: the spin–orbit ratios are lowest for scattering by Ar and higher for collisions with O_2 and CO. The spin–orbit ratio resulting from inelastic scattering is defined as "statistical" if the rotational and spin–orbit temperatures are equal. The spin–orbit ratios obtained in the inelastic scattering of NO by Ar are colder than statistical, but in collisions with CO and O_2 the resulting spin–orbit excitations, contrary to CID, are approximately statistical. Finally, the spin–orbit excitations appear to be much more sensitive to the nature of the collider than the rotational distributions.

IV. Discussion

In discussing the results obtained in this work, we use a statistical treatment rather than one based on microscopic state-to-state calculations. The justification for not using a microscopic approach is based on two factors. First, even though the initial excitation energy of NO_2* is well specified, the quantum state of NO_2* cannot be well defined. At energies approaching D_0, there are at least two strongly mixed electronic states of NO_2, $\tilde{X}^2A_1$ and $\tilde{A}^2B_2$, and the density of rovibronic states is sufficiently high (>1/cm^{-1}) that quantum mechanical effects in the collision energy transfer are not expected to be observed. Second, collisions create a broad distribution of excitation energies. In order to describe the collisional excitation and subsequent decomposition of those excited molecules (denoted NO_2*‡) whose internal energies exceed D_0 in a state-to-state manner, not only must the distribution of the NO_2*‡ excess energies, $E^\ddagger$, be known, but also the relevant cuts in the potential energy surfaces. This information is not yet available. Additionally, in our experiments possible fluctuations in the state-to-state energy transfer and decomposition rates will be averaged out, and therefore, knowing the state-specific details of the interaction potentials and reaction cross sections is less important. These considerations favor the use of a statistical treatment, where one starts from a microcanonical ensemble in NO_2* and describes CID by using an energy transfer law to obtain the distribution of decomposing states following collisional excitation.

1. Exponential Scaling of Collisional Energy Transfer Probability. An important conclusion derived from the CID yield spectra and the NO product state distributions is that the CID signal intensity scales exponentially with respect to the energy transferred per collision. Such exponential scaling of the probability has been observed previously[14] and is consistent with the empirical "energy gap law" for energy transfer.[35] This law has been independently formulated and used successfully in interpreting a large body of data for processes such as radiationless decay of excited electronic states (where the name energy gap law originates),[40–42] vibrational–translational and rotational–translational energy transfer in collisions of molecules, ions, and atoms.[3,43,44]

The exponential scaling of the CID signal suggests that the probability distribution $P(E_i,E_f)$ for transitions from initial internal energy level E_i to final energy E_f is given by the empirical equation

$$P(E_i,E_f) \propto \exp\left(-\frac{|E_f - E_i|}{\gamma}\right) \quad (8)$$

The parameter γ, which defines the scaling of the probability, depends on E_{col}, the microscopic properties of the colliders and the interaction potential. Typically, γ is different for activating and deactivating collisions,[35] but in the CID experiments only the activating collisions are monitored. For the activating collisions an upper limit of E_{col} must be placed on the total amount of energy that can be transferred from translational to internal degrees of freedom in the collisional system. This is taken into account by assuming that the transition probability is equal to zero when $(E_f - E_i) > E_{col}$.

Exponential scaling of the transition probability with the transferred energy is usually observed in adiabatic collisions. When the collision energy is large compared to the spacing between adjacent vibrational levels, the system can be treated semiclassically as a forced harmonic oscillator.[45] The transition probability can then be set proportional to the square of the Fourier component of the force acting during the collision at the frequency of the transition.[46,47] The collision is adiabatic when the duration of the collision exceeds the vibrational period. This assumption can be well justified, for instance, in the case of chattering collisions,[13] as well as in "sticky" collisions that involve formation of an intermediate collision complex.[4] In the latter case, however, if the lifetime of the intermediate is sufficiently long (e.g., many vibrational periods), a statistical distribution of the available energy within the complex may be achieved, and the product state distributions will be best predicted by considering the density of states of the entire collision system.[4] Therefore, an exponential scaling of the energy transfer probability is likely to be observed when the collisions are (*i*) long enough to satisfy the condition of adiabaticity (i.e., comparable to a vibrational period) and (*ii*) short enough to preclude randomization of the available energy within an intermediate complex.

Long-lived sticky or chattering collisions are unlikely in the CID of NO_2 due to the expected weakness of the NO_2*–collider interaction compared to E_{col}. The condition of adiabaticity may be satisfied at these collision energies, since the incident velocity (~1000 m·s^{-1}) does not exceed the velocity of the NO_2* vibrational motion (>2000 m·s^{-1}). However, the possibility of nonadiabatic collisions may increase at higher collision energies.

2. Unimolecular Decomposition Model of CID. When modeling the mechanism of CID, it is important to consider the nature of the interaction among the colliding species. In the simplest model, we assume that following collisional excitation of NO_2*, no further collider-product interaction occurs; in other words, the collider atom or molecule plays a spectator role in the NO_2 decomposition. The subsequent dissociation of collisionally excited NO_2*‡ can then be treated as a unimolecular reaction, and this mechanism will be referred to as the unimolecular decomposition (UMD) model. However, the possibility of some interaction with the collider in the exit channel (especially in the case of collisions with CO and O_2) cannot be ruled out *a priori* and may affect the NO energy partitioning. If NO_2*‡ decomposition occurs in the presence of the collider, then, strictly speaking, the collisionally excited

system can no longer be described in terms of isolated $NO_2^{*\ddagger}$. It may be more appropriate in this case to refer to the dissociating system as the O–NO–collider short-lived collisional complex, with the collider playing an active role in the energy partitioning (see below).

In the absence of such exit–channel interaction, T → V transfer leads to formation of $NO_2^{*\ddagger}$. Thus, if $h\nu$ is the initial excitation energy of NO_2^*, the probability of the $NO_2^*(h\nu) \rightarrow NO_2^{*\ddagger}(D_0 + E^\ddagger)$ transition is given by eq 8 with $E_i = h\nu$ and $E_f = D_0 + E^\ddagger$. Assuming that the density of states of NO_2 does not change significantly for $E^\ddagger = 0$–2400 cm^{-1}, the resulting population of $NO_2^{*\ddagger}$ for $(D_0 - h\nu) + E^\ddagger \leq E_{col}$ is

$$N_{NO_2}(E^\ddagger;h\nu) \propto I_{LIF}(h\nu) \exp\left(-\frac{(D_0 - h\nu) + E^\ddagger}{\gamma}\right) \quad (9)$$

where $I_{LIF}(h\nu)$ is the LIF intensity at $h\nu$, which is proportional to the intensity of the jet-cooled absorption feature at this energy.

Since $E^\ddagger$ is not directly observable and the CID signal is a result of integration over all energetically accessible $E^\ddagger$ levels, no definite conclusion can be drawn from the experimental data about the state-specific behavior of the energy transfer probability. As observed in the photodissociation of NO_2,[31] significant state-to-state fluctuations of the energy transfer cross section may be anticipated. However, because of averaging of the excited $NO_2^{*\ddagger}$ states whose energies lie above the threshold of the monitored NO product level, these fluctuations are not observed in the CID experiments. In addition, for every collision the state-specific transition probability is an average over initial conditions (i.e., impact parameter and orientation). Thus, eq 9 must be understood as an empirical law describing *on average* the collisional excitation of NO_2 in a reasonably narrow product energy interval where γ is constant. For the same reason, the local fluctuations in the $NO_2^{*\ddagger}$ density of states are not important.

In the absence of exit-channel interactions with the collider, the subsequent decomposition of $NO_2^{*\ddagger}$ can be described by phase space theory (PST) of unimolecular decay.[31,48–50] Before proceeding, we need to address the issue of collision-induced rotational excitation of $NO_2^{*\ddagger}$, since the collision transfers not only energy but also angular momentum which spreads the initially cold total angular momentum distribution ($T_{rot.} < 5$ K) over a wider range. As an estimate, we assume that the rotational temperature of $NO_2^{*\ddagger}$ is equal to the energy transfer parameter γ, which is of the order of 200 cm^{-1}. The rotational constant $\bar{B}$ of NO_2 near D_0 is calculated to be ~2–3 times less than that of the ground state NO_2 ($\bar{B}_0 = 0.43$ cm^{-1}).[51] Assuming $\bar{B} \approx 0.2$ cm^{-1}, we calculate that the average populated J_{NO_2}, corresponding to a rotational energy of ~200 cm^{-1}, is $\langle J_{NO_2} \rangle \sim 30.5$ (which is higher than the maximum observed J of NO in the CID experiments). Note that excitation of $J_{NO_2} \sim 30.5$ is allowed by angular momentum conservation. In the classical limit $|\boldsymbol{J}| = |\boldsymbol{L}|$ and $\mu v b$ where μ is the reduced mass of the NO_2–collider system, v is the relative velocity, and b is the impact parameter, excitation of $J_{NO_2} \sim 30.5$ corresponds to an impact parameter $b \sim 1$ Å. Since the range of the NO_2–collider interaction is significantly larger than 1 Å, collisional excitation of the NO_2 rotational states with $J_{NO_2} \sim 30.5$ or higher is feasible. Note, however, that the different dynamical constraints on the possible orientations of the NO J-vector for rotationally cold and hot $NO_2^{*\ddagger}$ that are used in PST do not affect the final results of the UMD computations as significantly as in the case of photodissociation of NO_2 at well selected energies. For example, no significant change in the outcome of the UMD model calculations was obtained when using $\langle J_{NO_2} \rangle = 8.5$.

The decomposition of $NO_2^{*\ddagger}$ is described here as a unimolecular reaction of rotationally hot NO_2. In applying angular momentum conservation under conditions where $J_{NO_2} > J_{NO}$, all possible orientations of the NO J-vector are allowed,[31] and the phase space available to each NO J-level is directly proportional to its degeneracy $(2J + 1)$. [Note that in this case the rotational degeneracy is similar to that obtained in a prior calculation.][31] Consequently, the density of the phase space allowed rotational states is the same as the total density of rotational states (including degeneracy); however, in the energy domain it is constant for both $NO(^2\Pi_{1/2})$ and $NO(^2\Pi_{3/2})$. In the present treatment we did not include any centrifugal constraints. In studies of the unimolecular reaction of NO_2 no cutoff in the NO rotational distributions due to centrifugal barriers was found,[31] giving a lower limit to the term due to the long range attraction between the O and NO products. Using this lower limit in the present calculations did not result in a significant change in the results compared to neglecting this term.

Statistically, at each $E^\ddagger$, $NO_2^{*\ddagger}$ decomposes to produce NO with equally populated energy levels $E_j \leq E^\ddagger$, where E_j is the total energy of the monitored NO state (rotational and spin–orbit). The corresponding contribution to the total CID yield of each NO energy level E_j is inversely proportional to the number $n(E^\ddagger)$ of NO quantum states that can be produced at this excess energy (i.e., states with $E_j < E^\ddagger$). Consequently, the contribution of $NO_2^{*\ddagger}$ in the narrow energy range between $E^\ddagger$ and $E^\ddagger + dE^\ddagger$ to the NO product state distribution at $E_j \leq E^\ddagger$ is

$$dN_\Omega(E_j,E^\ddagger;h\nu) = \varrho_\Omega(E_j)\frac{N_{NO_2}(E^\ddagger;h\nu)\,dE^\ddagger}{n(E^\ddagger)} \quad (10)$$

where $N_{NO_2}(E^\ddagger;h\nu)\,dE^\ddagger$ is the total number of $NO_2^{*\ddagger}$ molecules in the energy interval $dE^\ddagger$ produced by collisional excitation of $NO_2^*(h\nu)$. Thus, the CID yield per NO quantum state at energy interval $dE^\ddagger$ multiplied by the $NO(^2\Pi_\Omega)$ density of states $\varrho_\Omega(E_j)$ gives the yield of NO molecules with internal energy E_j in each spin–orbit state ($\Omega = {}^1/_2, {}^3/_2$). Substituting eq 9 into eq 10 we obtain

$$dN_\Omega(E_j,E^\ddagger;h\nu) \propto \frac{\varrho_\Omega(E_j)}{n(E^\ddagger)} I_{LIF}(h\nu) \exp\left(-\frac{(D_0 - h\nu) + E^\ddagger}{\gamma}\right) dE^\ddagger \quad (11)$$

As stated above, the density of NO states allowed by PST is constant in the rotational energy domain for both spin–orbit states. Thus, the product density of states is given by

$$\varrho_{1/2}(E_j) = \varrho_0, \quad \text{for } E_j > 0$$

$$\varrho_{3/2}(E_j) = 0, \quad \text{for } 0 < E_j < \epsilon_{s-o}$$

$$\varrho_{3/2}(E_j) = \varrho_0, \quad \text{for } E_j > \epsilon_{s-o} \quad (12)$$

where $\epsilon_{s-o} = 123$ cm^{-1} is the NO spin–orbit energy and ϱ_0 is a constant. The total NO density of states, $\varrho(E_j) = \varrho_{1/2}(E_j) + \varrho_{3/2}(E_j)$, is given by

$$\varrho(E_j) = \varrho_0, \quad \text{for } 0 < E_j < \epsilon_{s-o}$$

$$\varrho(E_j) = 2\varrho_0, \quad \text{for } E_j \geq \epsilon_{s-o} \quad (13)$$

The total number of states $n(E^{\ddagger})$ can be obtained by integrating $\varrho(E_j)$. $n(E^{\ddagger})$ is a linear function of $E^{\ddagger}$, but at $E^{\ddagger} = \epsilon_{s-o}$ its slope increases by a factor of 2, due to the opening of the $^2\Pi_{3/2}$ channel. Thus,

$$n(E^{\ddagger}) = \varrho_0 E^{\ddagger} \quad \text{for } E^{\ddagger} \le \epsilon_{s-o}$$

$$n(E^{\ddagger}) = \varrho_0(2E^{\ddagger} - \epsilon_{s-o}) \quad \text{for } E^{\ddagger} > \epsilon_{s-o} \qquad (14)$$

However, in reality $n(E^{\ddagger})$ is a steplike function of energy and cannot be <1 above D_0. The approximation in eq 14 is thus valid only when $n(E^{\ddagger})$ is significantly larger than 1.

To obtain the NO population as a function of product internal energy E_j and $h\nu$, eq 11 should be integrated over all the energetically accessible states $E^{\ddagger}$ above E_j. The use of integration is justified due to the high density of states of $NO_2{}^{*\ddagger}$. The NO state distribution depends parametrically on $h\nu$ and for each spin–orbit state ($\Omega = {}^1/_2, {}^3/_2$) is given by

$$N_\Omega(E;h\nu) \propto \int_{E_j}^{E_{col}-(D_0-h\nu)} \frac{\varrho_\Omega(E_j)}{n(E^{\ddagger})} I_{LIF}(h\nu) \times \exp\left(-\frac{(D_0 - h\nu) + E^{\ddagger}}{\gamma}\right) dE^{\ddagger} = I_{LIF}(h\nu) \exp\left(-\frac{D_0 - h\nu}{\gamma}\right) \varrho_\Omega(E_j)\, F(E_j;h\nu) \qquad (15)$$

where

$$F(E_j;h\nu) = \int_{E_j}^{E_{col}-(D_0-h\nu)} \frac{1}{n(E^{\ddagger})} \exp\left(-\frac{E^{\ddagger}}{\gamma}\right) dE^{\ddagger} \qquad (16)$$

while $\varrho_\Omega(E_j)$ and $n(E^{\ddagger})$ are given by eqs 12 and 14, respectively. Since $\varrho_{3/2}(E_j) = 0$ when $E_j < \epsilon_{s-o}$, it follows that $N_{3/2}(E_j;h\nu) = 0$ at these total energies.

Equations 15 and 16 enable the simulation of the CID state-specific yield spectra and the rotational distributions resulting from the UMD model. The simulation of the CID yield spectra is achieved by setting the lower limit of integration in eq 16 to the energy of the monitored NO($^2\Pi_{1/2}$;J=5.5) state, that is $E_j = 59$ cm^{-1}. Note, that when the upper limit of integration [$E_{col} - (D_0 - h\nu)$] exceeds the lower limit E_j by much more than γ, the integral becomes nearly independent of the upper limit (and, thus, of $h\nu$), since the integrand in the vicinity of the upper limit is exponentially small compared to its value near the lower limit. When this condition is satisfied, $F(E_j;h\nu)$ is nearly a constant for a given NO energy E_j. Thus, the CID yield spectrum at the excitation energies used in this study can be well represented by eq 2, which is equivalent to eq 15 if we set $F(E_j;h\nu)$ = constant. This is illustrated in Figure 11, where the thick curve is the $\ln(I_{CID}/I_{LIF})$ yield spectrum for NO ($^2\Pi_{1/2}$;J=5.5) calculated according to eqs 15 and 16 for the NO_2/He + Ar experiment. The straight thin line corresponds to eq 2 with the same γ parameter.

The CID yield of NO($^2\Pi_{1/2}$;J=5.5) changes rather smoothly (exponentially) when the energy available to the products significantly exceeds ($E_j + \gamma$). In this energy range the major factor leading to the decrease of the CID signal as $h\nu$ is scanned below D_0 is the exponential scaling of the energy transfer probability. The cutoff of the energy transfer at the value of the available energy [$E_{col} - (D_0 - h\nu)$] is not important experimentally, since the probability of excitation to this energy is very small compared to the probability of excitation to levels near the threshold of the NO(J=5.5) state. This explains why the CID yield spectra predicted by the UMD model and by eq 2, which does not take the energetic cutoff into account, are quite similar for a wide range of NO_2* excitation energies. However, when $h\nu$ is sufficiently low and the maximum $E^{\ddagger}$ is close to the threshold for production of NO($^2\Pi_{1/2}$;J=5.5), the cutoff region becomes important, since the number of $NO_2{}^{*\ddagger}$ states above E_j decreases rapidly with decreasing $h\nu$. This factor leads to a faster-than-exponential decrease of the CID signal and to the abrupt cutoff in the UMD curve shown in Figure 11.

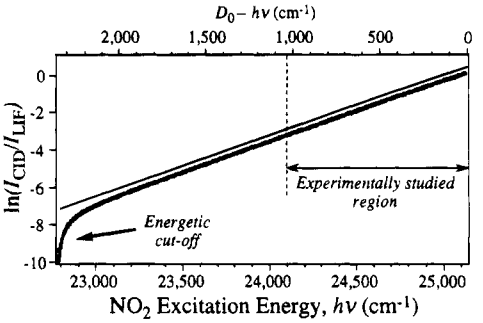

Figure 11. (Thick line) $\ln(I_{CID}/I_{LIF})$ calculated according to the UMD model. (Thin line) Similar curve calculated according to eq 2 [simple exponent] in which the cutoff at the available energy is neglected (see the text for details). In both cases, the monitored NO level for the CID spectrum is assumed to be the $^2\Pi_{1/2}$, J = 5.5 state (i.e., E_j = 59 cm^{-1}), E_{col} = 2400 cm^{-1}, and γ = 307 cm^{-1}. The separation between the linear part of the lines was introduced for clarity of presentation. Also indicated is the range of the excitation energies studied in the NO_2/He + Ar experiment.

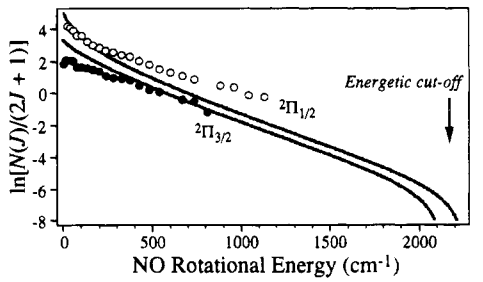

Figure 12. (Solid lines) Boltzmann plots of the NO($^2\Pi_{1/2}$,$^2\Pi_{3/2}$) rotational distributions calculated according to the UMD model with NO_2 excitation energy $D_0 - h\nu$ = 160 cm^{-1} (λ = 400.18 nm), E_{col} = 2400 cm^{-1}, and γ = 307 cm^{-1}. Boltzmann plots of the NO($^2\Pi_{1/2}$) and NO($^2\Pi_{3/2}$) rotational populations obtained in the NO_2/He + Ar experiment are shown as open and closed circles, respectively. Within each set (computational and experimental results), the rotational distributions of the two spin–orbit states are normalized correctly with respect to each other; however, the relative normalization of the experimental and computational results is arbitrary.

According to eq 15, the NO state distribution following excitation at energy $h\nu$ is proportional to the product of the integral in eq 16 and the density of states of the corresponding spin–orbit state. Boltzmann plots of the rotational distributions, plotted in the rotational energy domain (e.g., $E_{rot.} = E_j - \epsilon_{s-o}$ for $^2\Pi_{3/2}$) and calculated using the UMD model with E_{col} = 2400 cm^{-1}, ($D_0 - h\nu$) = 160 cm^{-1}, and γ = 307 cm^{-1} (i.e., the conditions of the NO_2/He + Ar experiment) are shown in Figure 12. Since large sections of the Boltzmann plots appear linear, a "rotational temperature" can be assigned to each distribution using the slope of its linear part.

3. Comparisons with Experimental Results. *(i) Average Energy Transferred per Collision.* The UMD model is in reasonable agreement with the observed exponential decay of the CID signal in the range of NO_2* energies studied in our experiments. The energetic cutoff of the CID signal at the available energy limit predicted by the UMD model (Figures 11 and 12) is not observed in the experiment, since the signals become too small to be measured. The values of the (upward)

energy transfer parameter γ obtained by fitting the experimental CID yield spectra using eq 2 are summarized in Table 2. Comparable values of the average energy transfer were obtained in the vibrational excitation and deactivation of $I_2(B)$ by collisions with He (100 cm^{-1})[52] and in the collisional deactivation of excited NO_2 with atomic and diatomic colliders.[7,9] In recent experiments, the average energy transfer for deactivating collisions of NO_2 excited at $h\nu = 20\,000$ cm^{-1} with Ar, CO, and O_2 was found to be 278, 558, and 238 cm^{-1}, respectively.[29] The energy transfer parameter is sensitive to the kinematic and microscopic properties of the collision system. Its dependence on collision energy is illustrated by the differences between the values obtained for collisions of NO_2* with Ar at two different E_{col} (Table 2). The dependence of γ on the nature of the collider is revealed by the fact that its value for the NO_2/He + Ar system (307 cm^{-1}) is 1.5−1.75 times larger than for the NO_2/He + CO and NO_2/He + O_2 systems (175 and 207 cm^{-1}, respectively). The corresponding collision energies are rather similar: 2400 *vs* 2200 and 2100 cm^{-1}, respectively. This dependence may reflect the greater stiffness of the atom collider as compared to a diatomic molecule. In the latter case, the additional degrees of freedom may absorb some of the collisional energy making the energy transfer to the internal degrees of freedom of NO_2* less efficient. A similar observation has been reported for CID on surfaces.[20c] Dependence of the microscopic properties of NO_2* on its excitation energy may also result in variation of γ with $h\nu$, although such variation is not observed in the CID yield spectra up to $D_0 - h\nu = 1000$ cm^{-1}.

In recent experiments, the relaxation of highly excited NO_2* by various colliders has been studied as a function of excitation energy.[6,7,9] Two points are relevant to the present CID studies: (*i*) even with molecular colliders (e.g., NO_2, CO_2, and N_2O) most of the relaxation proceeds via V → T transfer, and only a minority of the collisions (10−20%) result in V → V or V → R transfer; (ii) the average energy transferred per collision increases sharply when the NO_2* excitation energy exceeds ~10 000 cm^{-1}.

The first point suggests that most of the upward and downward energy transfer events involve small impact parameter collisions and that long-range resonant energy transfer is of secondary importance. However, the chemical interaction between the colliders may also be of importance and may even lead to chemical reactions. For example, the reactions NO_2* + CO → CO_2 + NO and NO_2* + O_2 → O_3 + NO are energetically allowed when the energy of NO_2* exceeds 9700 and 16 600 cm^{-1}, respectively.[53-55] We have looked for signatures of reactive scattering in the NO intensities and rotational distributions, but the results obtained with CO, O_2, and Ar colliders were not significantly different and thus no definite conclusion can be made about the participation of reactive channels. We note that the probability of the NO_2* + CO reaction has been found previously to be 2−3 orders of magnitude less than the NO_2* quenching probability,[56,57] which by microscopic reversibility is of the same order of magnitude as the CID probability at excitation energies just below D_0. However, even if reactive channels are of minor importance, chemical interactions between the colliders may govern the approach geometries, increase the tendency to create an intermediate complex, affect exit-channel interactions, or cause some rehybridization of orbitals. Thus, these systems may show greater sensitivity to the details of the interaction potential.

The second point raises the issue of the participation of excited electronic states of NO_2* in the energy transfer processes. The prepared eigenstates of NO_2* are known to be mixed $^2B_2/^2A_1$ states. In addition, other electronic states that are not accessed optically, namely, the $^2A_2$ and $^2B_1$ states, may be coupled collisionally. The electronic transition dipole moment is thought to mainly increase the efficiency of V−V transitions.[29] On the other hand, it is well-known that the strong mixings between the $^2B_2$ and $^2A_1$ states promote IVR, and, at the NO_2* excitation levels of our experiments, vibronic (and possibly rovibronic) chaos exists.[26] The existence of chaotic motions in the highly vibrationally excited NO_2* is probably responsible for the absence of state-specific effects in the CID yield spectra; except for the smooth exponential decrease in the CID spectral intensity as ($D_0 - h\nu$) increases, the LIF and CID yield spectra are identical.

(ii) Effect of Exit-Channel Interactions. The CID yield spectra calculated by the UMD model do not take account of final state interactions with the collider in the exit channel of dissociation (referred to as the exit-channel interaction) or of secondary collisions in the molecular beams intersection region. Such interactions are not expected to change the CID yield spectra significantly, since the collisional excitation step is not affected by exit-channel or collider-product interactions. On the other hand, the partitioning of excess energy between the CID products and the collider will be affected, and consequently, exit-channel interactions will be revealed predominantly in the product state distributions. The rotational temperatures and spin−orbit ratios obtained in our experiments and calculated according to the UMD model are listed in Tables 2 and 3. Values of γ obtained according to eq 2 were used in the UMD calculations. The rotational temperatures were obtained from the slopes of the linear parts of the NO rotational energy curves calculated by the UMD model (see Figure 12).

In general the NO spin−orbit excitations obtained in the CID experiments are colder than those predicted by the UMD model. The difference is especially noticeable in the NO_2/He + Ar experiment, for which both the UMD curve and the experimental data are depicted for comparison in Figure 12. The coldness of the observed NO spin−orbit ratio is not surprising since the same effect is observed in the collision-free unimolecular reaction of NO_2 (see Table 3).[31,58] As shown in Table 3, the calculated spin−orbit ratios would rise with increasing collision energy and/or γ. However, in the experiment they also appear to depend on the nature of the collider; for example, they are significantly hotter in collisions with CO and O_2 than in the NO_2/He + Ar collisions for which both E_{col} and γ are the largest. This suggests that in collisions with CO and O_2, exit-channel interactions may be important. However, the NO $^2\Pi_{1/2}$ and $^2\Pi_{3/2}$ rotational temperatures obtained by CID with different colliders are not significantly different. Although all the observed rotational distributions appear somewhat hotter than predicted by the UMD model, the differences between the different colliders can be accounted for merely by the differences in collision energies. Thus, the spin−orbit ratios appear to be more sensitive probes of exit-channel interactions.

Exit-channel interactions with the collider should be important if the collider is still in the vicinity of NO_2*‡ during dissociation. Since the lifetime of NO_2*‡ varies greatly with excess energy, we have to estimate the likelihood of an exit-channel interaction for collisions transferring large and small amounts of energy (efficient and inefficient collisions). For inefficient collisions, constituting the majority of all collisions and transferring ~300 cm^{-1} of energy at $E_{col} \sim 2000$ cm^{-1}, the relative exit-channel velocity is similar to the precollision velocity (<15 Å·ps^{-1}). The unimolecular decay lifetime of NO_2*‡ near threshold is ~5 ps,[59] yielding characteristic distances between the collider and NO_2*‡ molecule during dissociation of tens of angstroms. At

these distances no secondary interaction is possible. These estimates, however, do not take into account the possibility of chattering or sticky collisions or the formation of a collision complex. We have also overlooked the fact that the relative velocity of the colliders is smallest in the vicinity of the turning point (i.e., at the minimum separation). On the other hand, for efficient collisions, when the transferred energy is $(D_0 - h\nu + E^{\ddagger}) \sim 1000$ cm^{-1}, the relative exit-channel velocity is $\sim$10 Å·ps^{-1}. The dissociation lifetime of $NO_2{}^{*\ddagger}$ at $E^{\ddagger} \leq 1000$ cm^{-1} is estimated at $\geq$0.5 ps.[59] Thus, we find that the Ar$-NO_2{}^{*\ddagger}$ characteristic distance during dissociation will be of the order of only a few angstroms. Thus, some exit-channel interaction may occur, especially in those events for which the T $\rightarrow$ V transfer is large (leading to fast $NO_2{}^{*\ddagger}$ dissociation).

The absence of significant exit-channel interactions with the Ar collider is apparently a result of the weakness of the NO_2-Ar interaction compared to the collision energies employed in these experiments.[60,61] An NO_2 molecule colliding with Ar sees it, essentially, as a repulsive wall with a negligible attractive well preceding it. In the case of chemically active colliders such as CO or O_2, the interaction with the departing CID products, NO and O, is likely to be stronger and may affect the energy partitioning in the exit channel of the reaction.

Support for stronger exit-channel interactions with the CO and O_2 colliders, as compared with Ar, can be found in the results on inelastic scattering of background NO summarized in Table 4. Overall, compared to CID, a higher spin−orbit excitation of NO is observed. The general trend in NO spin−orbit excitations is the same as in CID: the ratios are lower for scattering by Ar and significantly higher for collisions with O_2 and CO. The spin−orbit ratios obtained in the inelastic scattering of NO by Ar are colder than statistical, and calculations show that they are dominated by repulsive interactions and sensitive to the difference potential.[62] Colder than statistical NO spin−orbit ratios are also observed in NO_2 photodissociation,[31] for which it is suggested that in the unimolecular decomposition of NO_2 rotational populations are fixed first, while the product spin−orbit ratio is determined later in the exit channel of dissociation at larger separation between NO and O.[58] This may explain why the spin−orbit populations in the CID experiment are more sensitive to the exit-channel interactions with the collider than the rotational distributions.

A second possible reason for deviations of the NO internal energy distributions from the predictions of the UMD model may involve secondary collisions in the beam. Although our experiments were performed under largely single-collision conditions, the actual number of collisions per molecule spans a broad distribution and some of the NO molecules produced by CID may undergo secondary collisions; of those $\sim$60% will be inelastic.[63] Simple estimates show that if the average number of collisions per molecule in the collision region (both elastic and inelastic) is $\sim$0.5, then almost 10% of the NO molecules produced by CID will undergo secondary collisions.

We expect that the effect of secondary collisions will be larger on the NO rotational distributions than on the spin−orbit ratios. Secondary collisions undergone even by a small number of CID NO products can significantly increase the population of rotational states in the tail of the distribution. The observed spin−orbit ratios, however, are less likely to be affected, since the relative cross sections of multiplet-changing transitions in inelastic scattering of NO by Ar are much smaller than the corresponding cross sections for multiplet-conserving transitions.[36] Since in our experiments deviations from the predictions of the UMD model are more noticeable in the spin−orbit distributions, we believe that secondary collisions are less important than exit-channel interactions with the collider during the dissociation.

Another possible reason for deviations from the UMD model may be the presence of clusters in the collider beam. The larger mass of a clustered collider increases the total relative collision energy, which tends to increase both the NO spin−orbit ratio and rotational temperature. However, the relative concentration of clusters in the collider beam is small compared to monomers, and signals due to cluster collisions are not expected to be observed, given our signal-to-noise ratio.

An analogy between the CID of $NO_2{}^*$ and the inelastic scattering of NO has also been noted in collisions with surfaces. The rotational distributions obtained in these two processes following collisions on MgO(100) single-crystal surfaces at collision energies comparable to those of the present study were similar.[21,64] An important distinction, however, is that the NO spin−orbit states produced in the surface collisions by both CID and inelastic scattering were nearly equally populated. These findings suggest that the nature of the interactions in the gas phase and on the surface are different. Equal population of the spin−orbit states in the surface CID experiments may indicate strong surface-product interactions and/or the nonadiabatic nature of the collisions.[21] Unfortunately, the small signals in the NO_2/MgO(100) CID experiment prevented a more detailed investigation of the CID mechanism, and the applicability of the exponential energy transfer law to the surface experiments was not established. In other surface-CID experiments, where larger molecules (e.g., *n*,*i*-C_3F_7NO) were collisionally dissociated on MgO(100) at high incident energies ($\leq$7 eV), the observed NO product spin−orbit ratio was $\sim$0.3−0.4, similar to the ratio obtained in the gas-phase unimolecular reactions of these molecules, suggesting that the (slower) unimolecular dissociation of the larger molecules occurred far from the surface and thus secondary interactions were absent.[20b]

V. Summary

1. The CID of $NO_2{}^*$ with Ar, CO, and O_2 is an efficient process when the $NO_2{}^*$ excitation energy approaches D_0. The CID yield at excitation energies just below D_0 is $\sim$5% of the NO_2 photodissociation yield just above D_0 and decreases exponentially when the energy required to reach D_0 increases.

2. The average energy transferred per activating collision obtained in CID, 100−300 cm^{-1}, is comparable to the values obtained in the collisional deactivation of $NO_2{}^*$ with atomic and diatomic colliders.

3. The main trends in the experimental results, that is, CID yield spectra and NO spin−orbit and rotational energy distributions, can be explained by assuming a collisional activation step obeying an exponential gap law, followed by unimolecular decomposition of $NO_2{}^{*\ddagger}$ molecules (i.e., those molecules whose energy exceeds D_0).

4. A dependence of the CID on the nature of the collider is observed and is revealed mainly in the NO spin−orbit ratios. Some exit-channel interaction with the collider is suggested.

5. No indication of reactive scattering in collisions of $NO_2{}^*$ with CO and O_2 is revealed.

Acknowledgment. We thank M. Hunter for help in the early stage of these experiments, S. A. Reid for help in the measurement of the NO_2 LIF spectrum, C. Wittig, S. A. Reid, W. R. Gentry, and H. Ferkel for valuable discussions, and G. W. Flynn, H.-L. Dai, G. V. Hartland, and R. G. Gilbert for sending their results prior to publication. This work is supported by the Army Research Office and the National Science Foundation.

References and Notes

(1) (a) Forst, W. *Theory of Unimolecular Reactions*; Academic: New York, 1973. (b) Robinson, P. J.; Holbrook, K. A. *Unimolecular Reactions*; Wiley: New York, 1972. (c) Gilbert, R. G.; Smith, S. C. *Theory of Unimolecular and Recombination Reactions*; Blackwell Scientific: Oxford, U.K., 1990.

(2) Lindemann, F. A. *Trans. Faraday Soc.* **1922**, *17*, 598.

(3) Yardley, J. T. *Introduction to Molecular Energy Transfer*; Academic Press: New York, 1980.

(4) Flynn, G. W.; Weston, R. E., Jr. *J. Phys. Chem.* **1993**, *97*, 8116.

(5) Donnelly, V. M.; Keil, D. G.; Kaufman, F. *J. Chem. Phys.* **1979**, *71*, 659.

(6) (a) Chou, J. Z.; Hewitt, S. A.; Hershberger, J. F.; Brady, B. B.; Spector, G. B.; Chia, L.; Flynn, G. W. *J. Chem. Phys.* **1989**, *91*, 5392. (b) Chou, J. Z.; Hewitt, S. A.; Hershberger, J. F.; Flynn, G. W. *J. Chem. Phys.* **1990**, *93*, 8474.

(7) Toselli, B. M.; Walunas, T. L.; Barker, J. R. *J. Chem. Phys.* **1990**, *92*, 4793.

(8) Patten, K. O., Jr.; Johnston, H. S. *J. Phys. Chem.* **1993**, *97*, 9904.

(9) Hartland, G. V.; Qin, D.; Dai, H.-L. *J. Chem. Phys.* **1994**, *100*, 7832.

(10) Hase, W. L.; Date, N.; Bhuiyan, L. B.; Buckowski, D. G. *J. Phys. Chem.* **1985**, *89*, 2502.

(11) (a) Hippler, H.; Schranz, H. W.; Troe, J. *J. Phys. Chem.* **1986**, *90*, 6158. (b) Schranz, H. W.; Troe, J. *J. Phys. Chem.* **1986**, *90*, 6168.

(12) (a) Bruehl, M.; Schatz, G. *J. Chem. Phys.* **1988**, *89*, 770. (b) Bruehl, M.; Schatz, G. *J. Phys. Chem.* **1988**, *92*, 7223. (c) Lendvay, G.; Schatz, G. *J. Phys. Chem.* **1990**, *94*, 8864. (d) Lendvay, G.; Schatz, G. *J. Phys. Chem.* **1991**, *95*, 8748. (e) Lendvay, G.; Schatz, G. *J. Chem. Phys.* **1992**, *96*, 4356.

(13) Gilbert, R. G. *Int. Rev. Phys. Chem.* **1991**, *10*, 319.

(14) Oref, I.; Tardy, D. C. *Chem. Rev.* **1990**, *90*, 1407.

(15) Galucci, C. R.; Schatz, G. C. *J. Phys. Chem.* **1982**, *86*, 2352.

(16) (a) Tully, F. P.; Lee, Y. T.; Berry, R. S. *Chem. Phys. Lett.* **1971**, *9*, 80. (b) Tully, F. P.; Cheung, W. H.; Haberland, H.; Lee, Y. T. *J. Chem. Phys.* **1980**, *73*, 4460.

(17) Parks, E. K.; Pobo, L. G.; Wexler, S. *J. Chem. Phys.* **1984**, *80*, 5003.

(18) Smedley, J. E.; Haugen, H. K.; Leone, S. R. *J. Chem. Phys.* **1987**, *86*, 6801.

(19) (a) Kolodney, E.; Amirav, A. In *Dynamics on Surfaces*; Pullman, B., Jortner, J., Nitzan, A., Gerber, R. B., Eds.; Reidel: Dordrecht, The Netherlands, 1984; Vol. 17, p 231. (b) Kolodney, E.; Amirav, A.; Elber, R.; Gerber, R. B. *Chem. Phys. Lett.* **1984**, *111*, 366. (c) Kolodney, E.; Amirav, A.; Elber, R.; Gerber, R. B. *Chem. Phys. Lett.* **1985**, *113*, 303. (d) Gerber, R. B.; Amirav, A. *J. Phys. Chem.* **1986**, *90*, 4483. (e) Danon, A.; Kolodney, E.; Amirav, A. *Surf. Sci.* **1988**, *193*, 132. (f) Danon, A.; Amirav, A. *J. Phys. Chem.* **1989**, *93*, 5549.

(20) (a) Kolodney, E.; Baugh, D.; Powers, P. S.; Reisler, H.; Wittig, C. *J. Chem. Phys.* **1989**, *90*, 3883. (b) Kolodney, E.; Powers, P. S.; Hodgson, L.; Reisler, H.; Wittig, C. *J. Chem. Phys.* **1991**, *94*, 2330. (c) Powers, P. S.; Kolodney, E.; Hodgson, L.; Ziegler, G.; Reisler, H.; Wittig, C. *J. Phys. Chem.* **1991**, *95*, 8387.

(21) Ferkel, H.; Singleton, J. T.; Reisler, H.; Wittig, C. *Chem. Phys. Lett.* **1994**, *221*, 447.

(22) Bieler, C. R.; Sanov, A.; Hunter, M.; Reisler, H. *J. Phys. Chem.* **1994**, *98*, 1058.

(23) (a) Robra, U.; Zacharias, H.; Welge, K. *Z. Phys. D* **1990**, *16*, 175. (b) Chen, C. H.; Clark, D. W.; Payne, M. G.; Kramer, S. D. *Opt. Commun.* **1980**, *32*, 391. (c) Butenhoff, T. J.; Rohlfing, E. A. *J. Chem. Phys.* **1993**, *98*, 5460.

(24) (a) Haller, E.; Köppel, H.; Cederbaum, L. S. *J. Mol. Spectrosc.* **1985**, *111*, 377. (b) Köppel, H.; Domcke, W.; Cederbaum, L. S. *Adv. Chem. Phys.* **1984**, *57*, 59.

(25) Lehmann, K. K.; Coy, S. L. *Ber. Bunsen-Ges. Phys. Chem.* **1988**, *92*, 306.

(26) (a) Delon, A.; Jost, R. *J. Chem. Phys.* **1991**, *95*, 5686. (b) Delon, A.; Jost, R.; Lombardi, M. *J. Chem. Phys.* **1991**, *95*, 5701.

(27) (a) Douglas, A. E.; Huber, K. P. *Can. J. Phys.* **1965**, *43*, 74. (b) Douglas, A. E. *J. Chem. Phys.* **1966**, *45*, 1007.

(28) Patten, K. O., Jr.; Burley, J. D.; Johnston, H. S. *J. Phys. Chem.* **1990**, *94*, 7960.

(29) Hartland, G. V.; Qin, D.; Dai, H.-L. Private communication.

(30) Proch, D.; Trickl, J. *Rev. Sci. Instrum.* **1989**, *60*, 713.

(31) Hunter, M.; Reid, S. A.; Robie, D. C.; Reisler, H. *J. Chem. Phys.* **1993**, *99*, 1093.

(32) Kolodney, E.; Amirav, A. *Chem. Phys.* **1983**, *82*, 269.

(33) (a) Miller, J. C.; Compton, R. N. *Chem. Phys.* **1981**, *75*, 22. (b) Jacobs, D. C.; Zare, R. N. *J. Chem. Phys.* **1986**, *85*, 5457. (c) Wiley, W. C.; McLaren, I. H. *Rev. Sci. Instrum.* **1955**, *26*, 1150.

(34) (a) Busch, G. E.; Wilson, K. R. *J. Chem. Phys.* **1972**, *56*, 3626. (b) Busch, G. E.; Wilson, K. R. *J. Chem. Phys.* **1972**, *56*, 3638.

(35) Troe, J. *J. Chem. Phys.* **1977**, *66*, 4745.

(36) Joswig, H.; Andresen, P.; Schinke, R. *J. Chem. Phys.* **1986**, *85*, 1904.

(37) Jons, S. D.; Shirley, J. E.; Vonk, M. T.; Giese, C. F.; Gentry, W. R. *J. Chem. Phys.* **1992**, *97*, 7831.

(38) Bontuyan, L. S.; Suits, A. G.; Houston, P. L.; Whitaker, B. J. *J. Phys. Chem.* **1993**, *97*, 6342.

(39) Bieler, C. R.; Sanov, A.; Reisler, H. *Chem. Phys. Lett.*, in press.

(40) Kober, E. M.; Caspar, J. V.; Lipkin, R. S.; Meyer, T. J. *J. Phys. Chem.* **1986**, *90*, 3722.

(41) Lipkin, R. S.; Meyer, T. J. *J. Phys. Chem.* **1986**, *90*, 5307.

(42) Wagner, B. D.; Tittelbach-Helmrich, D.; Steer, R. P. *J. Phys. Chem.* **1992**, *96*, 7904.

(43) Hippler, H.; Troe, J. In *Advances in Gas-Phase Photochemistry and Kinematics: Bimolecular Collisions*; Ashfold, M. N. R., Baggott, J. E., Eds.; The Royal Society of Chemistry: London, 1989; pp 209–262.

(44) Brunner, T. A.; Pritchard, D. In *Dynamics of the Excited State*; Lawley, K. P., Ed.; Wiley: New York, 1982; p 589.

(45) Ma, Z.; Jons, S. D.; Giese, C. F.; Gentry, W. R. *J. Chem. Phys.* **1991**, *94*, 8608.

(46) Landau, L. *Phys. Z. Sowjetunion* **1932**, *1*, 88.

(47) Landau, L.; Teller, E. *Phys. Z. Sowjetunion* **1936**, *10*, 34.

(48) (a) Pechukas, P.; Light, J. C.; Rankin, C. *J. Chem. Phys.* **1966**, *44*, 794. (b) Pechukas, P.; Light, J. C. *J. Chem. Phys.* **1965**, *42*, 3281.

(49) Light, J. C. *Discuss. Faraday Soc.* **1967**, *44*, 14.

(50) (a) Klotz, C. E. *J. Phys. Chem.* **1971**, *75*, 1526. (b) Klotz, C. E. *Z. Naturforsch. A* **1972**, *27*, 553.

(51) Harding, L. B. Private communication.

(52) (a) Krajnovich, D. J.; Butz, K. W.; Du, H.; Parmenter, C. S. *J. Chem. Phys.* **1989**, *91*, 7705. (b) Krajnovich, D. J.; Butz, K. W.; Du, H.; Parmenter, C. S. *J. Chem. Phys.* **1989**, *91*, 7725.

(53) (a) Calhoun, G. M.; Crist, R. H. *J. Chem. Phys.* **1937**, *5*, 301. (b) Brown, F. B.; Crist, R. H. *J. Chem. Phys.* **1941**, *9*, 840.

(54) Johnston, H. S.; Bonner, W. A.; Wilson, D. J. *J. Chem. Phys.* **1957**, *26*, 1002.

(55) Thomas, J. H.; Woodman, G. R. *Trans. Faraday Soc.* **1967**, *63*, 2728.

(56) Herman, I. P.; Mariella, R. P., Jr.; Javan, A. *J. Chem. Phys.* **1978**, *68*, 1070.

(57) Umstead, M. E.; Lloyd, S. A.; Lin, M. C. *Appl. Phys. B* **1986**, *39*, 55.

(58) Reid, S. A.; Robie, D. C.; Reisler, H. *J. Chem. Phys.* **1994**, *100*, 4256.

(59) Ionov, S. I.; Brucker, G. A.; Jaques, C.; Chen, Y.; Wittig, C. *J. Chem. Phys.* **1993**, *99*, 3420.

(60) Nielson, G. C.; Parker, G. A.; Pack, R. T. *J. Chem. Phys.* **1977**, *66*, 1396.

(61) Alexander, M. H. *J. Chem. Phys.* **1993**, *99*, 7725.

(62) Alexander, M. H. *J. Chem. Phys.* **1982**, *76*, 5974.

(63) Thuis, H.; Stolte, S.; Reuss, J. *Chem. Phys.* **1979**, *43*, 351.

(64) Kolodney, E.; Baugh, D.; Powers, P. S.; Reisler, H.; Wittig, C. *Chem. Phys. Lett.* **1988**, *145*, 177.

JP941912O